Progress In Electromagnetics Research, PIER 67, 135–152, 2007

ANALYSIS OF RADIATION FROM A CYLINDRICAL-RECTANGULAR MICROSTRIP PATCH ANTENNA LOADED WITH A SUPERSTRATE AND AN AIR GAP, USING THE ELECTRIC SURFACE CURRENT MODEL

F. R. Cooray and J. S. Kot

CSIRO ICT Centre
P. O. Box 76, Epping, NSW 1710, Australia

Abstract—Radiation from a superstrate loaded cylindrical-rectangular microstrip patch antenna with an air gap between the substrate and the superstrate, is analyzed using the full-wave approach and the electric surface current model. Results are presented in the form of normalized radiation patterns for various thicknesses of the air gap and also for superstrates made of lossy dielectric material, to show the effects of these on the radiation from the antenna. Both axial and azimuthal current elements are considered.

1. INTRODUCTION

Microstrip patch antennas are widely used as conformal antennas in many practical applications. When a microstrip patch antenna is employed as an outdoor antenna, a superstrate layer is generally added on top of the patch to act as a radome to provide protection from environmental hazards such as rain, snow, dirt, etc. As the addition of a superstrate layer can change the characteristics of the microstrip structure, being able to analyze a microstrip antenna loaded with a superstrate is vital to understand how the radiation from it would change with the type of superstrate being used.

Since the cylindrical-rectangular microstrip patch antenna is a very popular type of conformal antenna, it has been analyzed in the past using different methods. In [1, 2], the cavity model has been used to analyze cylindrical-rectangular patch antennas, printed on a dielectric substrate, while in [3, 4] the method of moments (MoM) has been used for analyzing them. Similar antennas printed on a chiral substrate have been analyzed in [5] using the MoM and the

dyadic Green's functions derived for the problem with reference to [6, 7]. The MoM has been used in [8, 9] also, but for analyzing a cylindrical-rectangular patch antenna loaded with a lossless dielectric superstrate. The analysis of a cylindrical-rectangular microstrip patch antenna using the electric surface current model (ESCM) was first presented in [10, 11], with the main emphasis being to calculate the radiation from the antenna. Recently, such an antenna loaded with a lossless dielectric superstrate and fed by a coaxial probe is supposed to have been analyzed in [12] using the ESCM, but no details of the analysis have been given. The main advantage of using the ESCM is being able to obtain a closed form solution. As such, the analysis is simpler and the time taken for performing the analysis is much less than that when using the MoM. Also, the ESCM can be used to analyze a patch antenna loaded with a superstrate directly on top or spaced away from the patch with an air gap, for which the cavity model cannot be used.

In this paper, we analyze a cylindrical-rectangular microstrip patch antenna loaded with a superstrate spaced away from the patch and an air gap between the substrate and the superstrate, using the ESCM, for superstrates made of lossy dielectric material, to investigate the effects of the thickness of the air gap and the lossyness of the superstrate material on the radiation from the antenna. The antenna is modeled using an infinitely long concentric circular cylindrical microstrip structure consisting of a perfectly conducting ground cylinder and coaxial cylindrical substrate, air gap, and superstrate layers. The patch is assumed to be a perfect conductor of zero thickness printed on the dielectric substrate. In order to perform the analysis, the patch is replaced by an assumed surface current distribution, which in many cases can be obtained using a cavity model approximation that is valid as long as the radiation is small compared to the stored energy. To the best of the authors' knowledge, this is the first time a detailed analysis of such a structure using the ESCM has been presented.

The structure of the rest of the paper is as follows. Section 2 describes the formulation of the problem which is carried out by expressing the electromagnetic fields in each region in terms of a two-dimensional inverse Fourier transform with unknown expansion coefficients and then imposing the appropriate boundary conditions at each interface between regions. The evaluation of the fields in the far zone is described in Section 3, and the results obtained in the form of normalized radiation patterns and directivity patterns for different thicknesses of the air gap as well as for superstrate materials of different permittivities are given in Section 4. Finally, some conclusions are presented in Section 5.

2. FORMULATION

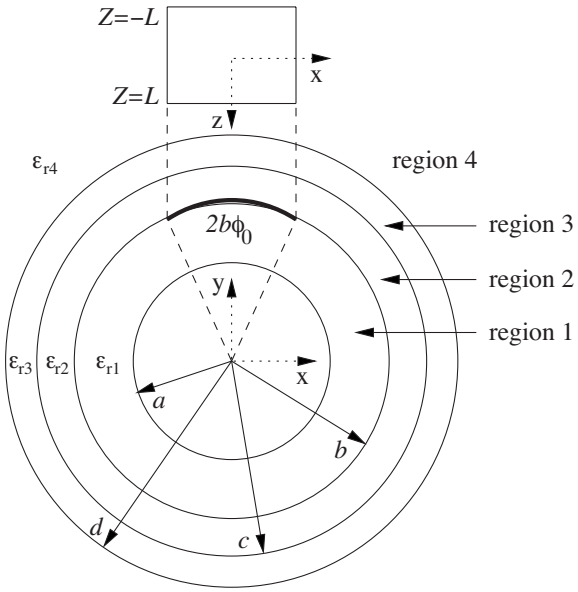

Figure 1. Geometry of the cylindrical-rectangular microstrip antenna loaded with a superstrate and an air gap between the substrate and the superstrate.

Consider a cylindrical-rectangular microstrip patch antenna loaded with a dielectric superstrate and an air gap between the substrate and the superstrate, as shown in Fig. 1. The microstrip patch is mounted on an infinitely long cylindrical ground of radius a. The cylindrical substrate (region 1) has a relative permittivity ϵ_{r1} and a thickness $b-a$, the air gap (region 2) has a relative permittivity $\epsilon_{r2}=1$ and a thickness $c-b$, while the cylindrical superstrate (region 3) has a relative permittivity ϵ_{r3} and a thickness $d-c$. Region 4 is free space with permittivity ϵ_0 or relative permittivity $\epsilon_{r4}=1$. The permeability in all regions is assumed to be free space permeability μ_0. The curved rectangular patch located at the substrate-air gap interface has a straight dimension $2L$ and a curved dimension $2b\phi_0$ as shown in Fig. 1, with $2\phi_0$ being the angle subtended by the curved patch at the center of the coaxial cylinders. Assuming a time harmonic dependence of $\exp(j\omega t)$, the z components of the electric and magnetic fields in the ith region for $i=1,2,3,4$ can be expressed in terms of functions in a cylindrical coordinate system (ρ,ϕ,z) attached to the center of the

coaxial cylinders as [13]

$$E_{iz}(\rho,\phi,z)=\frac{1}{2\pi}\sum_{n=-\infty}^{\infty}e^{jn\phi}\int_{-\infty}^{\infty}dk_z\,e^{-jk_zz}[A_{in}H_n^{(2)}(k_{i\rho}\rho)+B_{in}J_n(k_{i\rho}\rho)] \tag{1}$$

$$H_{iz}(\rho,\phi,z)=\frac{1}{2\pi}\sum_{n=-\infty}^{\infty}e^{jn\phi}\int_{-\infty}^{\infty}dk_z\,e^{-jk_zz}[C_{in}H_n^{(2)}(k_{i\rho}\rho)+D_{in}J_n(k_{i\rho}\rho)] \tag{2}$$

where k_z is the propagation constant, $k_{i\rho}^2=\omega^2\mu_0\epsilon_i-k_z^2$, $\epsilon_i=\epsilon_0\epsilon_{ri}$, $A_{in}, B_{in}, C_{in}, D_{in}$ are the unknown expansion coefficients of harmonic order n and functions of k_z, and $H_n^{(2)}(x)$, $J_n(x)$ are respectively, the Hankel function of the second kind and the Bessel function, of order n and argument x. The transverse field components $E_{i\rho}$, $E_{i\phi}$, $H_{i\rho}$, $H_{i\phi}$ in the ith region can be obtained from E_{iz} and H_{iz} as [14]

$$E_{i\rho}=-\frac{jk_z}{k_{i\rho}^2}\frac{\partial E_{iz}}{\partial\rho}-\frac{j\omega\mu_0}{k_{i\rho}^2\rho}\frac{\partial H_{iz}}{\partial\phi},\quad E_{i\phi}=-\frac{jk_z}{k_{i\rho}^2\rho}\frac{\partial E_{iz}}{\partial\phi}+\frac{j\omega\mu_0}{k_{i\rho}^2}\frac{\partial H_{iz}}{\partial\rho} \tag{3}$$

$$H_{i\rho}=\frac{j\omega\epsilon_i}{k_{i\rho}^2\rho}\frac{\partial E_{iz}}{\partial\phi}-\frac{jk_z}{k_{i\rho}^2}\frac{\partial H_{iz}}{\partial\rho},\quad H_{i\phi}=-\frac{j\omega\epsilon_i}{k_{i\rho}^2}\frac{\partial E_{iz}}{\partial\rho}-\frac{jk_z}{k_{i\rho}^2\rho}\frac{\partial H_{iz}}{\partial\phi}. \tag{4}$$

To solve for the unknown expansion coefficients, appropriate boundary conditions for the tangential field components should be imposed at the interfaces $\rho=a$, b, c, d. Imposing the boundary conditions $E_{1z}=0$ and $E_{1\phi}=0$ at $\rho=a$ yield

$$F(A_{1n},B_{1n},k_{1\rho},a)=0 \tag{5}$$

$$\frac{nk_z}{k_{1\rho}^2a}F(A_{1n},B_{1n},k_{1\rho},a)+\frac{j\omega\mu_0}{k_{1\rho}}F'(C_{1n},D_{1n},k_{1\rho},a)=0 \tag{6}$$

where

$$F(P_{in},Q_{in},k_{i\rho},\rho)=P_{in}H_n^{(2)}(k_{i\rho}\rho)+Q_{in}J_n(k_{i\rho}\rho)$$

$$F'(P_{in},Q_{in},k_{i\rho},\rho)=P_{in}H_n^{(2)'}(k_{i\rho}\rho)+Q_{in}J_n'(k_{i\rho}\rho)$$

for $i=1,2,3,4$, with $H_n^{(2)'}(x)$ and $J_n'(x)$ denoting the respective derivatives of $H_n^{(2)}(x)$ and $J_n(x)$, with respect to x.

The equations obtained by imposing the boundary conditions for E_{iz} and $E_{i\phi}$ at each of the interfaces $\rho=b$, $\rho=c$, and $\rho=d$ can be written in the general form

$$\sum_{i=p}^{p+1}(-1)^iF(A_{in},B_{in},k_{i\rho},\varrho)=0 \tag{7}$$

$$\sum_{i=p}^{p+1}(-1)^i\left\{\frac{nk_z}{k_{i\rho}^2\varrho}F(A_{in},B_{in},k_{i\rho},\varrho)+\frac{j\omega\mu_0}{k_{i\rho}}F'(C_{in},D_{in},k_{i\rho},\varrho)\right\}=0 \tag{8}$$

with $B_{4n}=D_{4n}=0$, and the two equations associated with each of the interfaces $\rho=b$, $\rho=c$, and $\rho=d$ obtained by substituting $p=1$ $\varrho=b$, $p=2$ $\varrho=c$, and $p=3$ $\varrho=d$, respectively, in (7) and (8).

The general form of the equations resulting from imposing the boundary conditions for H_{iz} and $H_{i\phi}$ at each of the interfaces $\rho=c$ and $\rho=d$ can be obtained from (7) and (8), respectively, by replacing A_{in},B_{in} by C_{in},D_{in} and vice versa, and replacing μ_0 by $-\epsilon_i$.

A_{in}, B_{in}, C_{in}, D_{in} for $i=1,2,3$ can then be expressed in terms of A_{4n} and C_{4n} using the above equations that resulted from imposing the boundary conditions for the tangential electric and magnetic fields as

$$C_{in} = \sigma_i^a A_{4n}+\sigma_i^c C_{4n} \tag{9}$$
$$D_{in} = \tau_i^a A_{4n}+\tau_i^c C_{4n} \tag{10}$$
$$A_{in} = \alpha_i^a A_{4n}+\alpha_i^c C_{4n} \tag{11}$$
$$B_{in} = \beta_i^a A_{4n}+\beta_i^c C_{4n} \tag{12}$$

with σ_i^e, τ_i^e, α_i^e, β_i^e for $i=1,2,3$, $e=a,c$ defined in Appendix A.

By applying the discontinuity boundary condition $\hat{\boldsymbol{\rho}}\times(\boldsymbol{H}_2-\boldsymbol{H}_1)=\boldsymbol{J}$ at $\rho=b$, where $\boldsymbol{H}_i$ is the magnetic field in region i and $\boldsymbol{J}$ is the surface current on the patch, we get $H_{1z}-H_{2z}=J_\phi$, $H_{2\phi}-H_{1\phi}=J_z$. Substituting for H_{1z}, H_{2z} from (2) and for $H_{1\phi}$, $H_{2\phi}$ from (4), and then taking the Fourier transforms of both sides of the equations yield

$$\tilde{J}_\phi(n,k_z)=\sum_{i=1}^{2}(-1)^{i-1}F(C_{in},D_{in},k_{i\rho},b) \tag{13}$$

$$\tilde{J}_z(n,k_z)=\sum_{i=1}^{2}(-1)^{i-1}\left[\frac{j\omega\epsilon_i}{k_{i\rho}}F'(A_{in},B_{in},k_{i\rho},b)-\frac{nk_z}{k_{i\rho}^2 b}F(C_{in},D_{in},k_{i\rho},b)\right] \tag{14}$$

where

$$\tilde{J}_\zeta(n,k_z)=\frac{1}{2\pi}\int_{-\pi}^{\pi}d\phi\int_{-\infty}^{\infty}dz\,J_\zeta(\phi,z)\,e^{-jn\phi}e^{jk_z z}. \tag{15}$$

The two equations obtained by substituting from (9)–(12) in (13) and (14) can be written in a matrix form as

$$\begin{bmatrix}\tilde{J}_z(n,k_z)\\ \tilde{J}_\phi(n,k_z)\end{bmatrix}=\begin{bmatrix}M_{11}(n,k_z) & M_{12}(n,k_z)\\ M_{21}(n,k_z) & M_{22}(n,k_z)\end{bmatrix}\begin{bmatrix}A_{4n}\\ C_{4n}\end{bmatrix} \tag{16}$$

in which

$$M_{11}(n,k_z) = \sum_{i=1}^{2}(-1)^{i-1}\left\{\frac{j\omega\epsilon_i}{k_{i\rho}}[\alpha_i^a H_n^{(2)'}(k_{i\rho}b)+\beta_i^a J_n'(k_{i\rho}b)] - \frac{nk_z}{k_{i\rho}^2 b}[\sigma_i^a H_n^{(2)}(k_{i\rho}b)+\tau_i^a J_n(k_{i\rho}b)]\right\} \quad (17)$$

$$M_{21}(n,k_z) = \sum_{i=1}^{2}(-1)^{i-1}\,[\sigma_i^a H_n^{(2)}(k_{i\rho}b)+\tau_i^a J_n(k_{i\rho}b)]. \quad (18)$$

Explicit expressions of $M_{12}(n,k_z)$ and $M_{22}(n,k_z)$ can be obtained from (17) and (18), respectively, by replacing α_i^a, β_i^a, τ_i^a, and σ_i^a by α_i^c, β_i^c, τ_i^c, and σ_i^c, respectively.

Equation (16) can now be solved to yield

$$A_{4n}(k_z) = \frac{M_{22}(n,k_z)}{\Delta(n,k_z)}\tilde{J}_z(n,k_z) - \frac{M_{12}(n,k_z)}{\Delta(n,k_z)}\tilde{J}_\phi(n,k_z) \quad (19)$$

$$C_{4n}(k_z) = -\frac{M_{21}(n,k_z)}{\Delta(n,k_z)}\tilde{J}_z(n,k_z) + \frac{M_{11}(n,k_z)}{\Delta(n,k_z)}\tilde{J}_\phi(n,k_z) \quad (20)$$

where we have shown explicitly the dependence of A_{4n} and C_{4n} on k_z, and

$$\Delta(n,k_z) = M_{11}(n,k_z)M_{22}(n,k_z) - M_{12}(n,k_z)M_{21}(n,k_z).$$

3. RADIATED FIELDS

Expressions for the axial and azimuthal components of the electric field in the region exterior to the coaxial cylinders can be obtained by substituting $i = 4$ in (1) and (3), respectively. The expressions of these field components in the far zone transverse to the radial direction can then be obtained from the above by using the asymptotic expressions for the Hankel functions [13] and evaluating the resulting infinite integrals over k_z using the saddle point method [15] as

$$E_\theta(r,\theta,\phi) = -\frac{1}{\sin\theta}\frac{e^{-jk_0 r}}{\pi r}\sum_{n=-\infty}^{\infty} j^{n+1}e^{jn\phi}\,A_{4n}(k_0\cos\theta) \quad (21)$$

$$E_\phi(r,\theta,\phi) = \frac{\eta_0}{\sin\theta}\frac{e^{-jk_0 r}}{\pi r}\sum_{n=-\infty}^{\infty} j^{n+1}e^{jn\phi}\,C_{4n}(k_0\cos\theta) \quad (22)$$

where r,θ,ϕ are the spherical coordinates of the field point with respect to an origin located at the center of the coaxial cylinders, k_0 is the free space wavenumber and η_0 is the free space wave impedance.

3.1. Radiation from an Axial Patch Antenna

In this case we consider the patch dimensions $2L$ and $2b\phi_0$ in Fig. 1 to be equal to half a wavelength and the patch width w, respectively, and the surface current $\boldsymbol{J}_s$ on the patch to be axially directed. Assuming the variation of $\boldsymbol{J}_s$ with the azimuthal coordinate ϕ to be negligible, it can be written in terms of an effective relative permittivity ϵ_{eff} as [11]

$$\boldsymbol{J}_s(\phi, z) = \begin{cases} \hat{\boldsymbol{z}} \dfrac{I_0}{w} \cos(k_0 \sqrt{\epsilon_{\text{eff}}} z), & -\bar{\lambda}_0 \le z \le \bar{\lambda}_0, \ \ -\phi_0 \le \phi \le \phi_0 \\ 0, & \text{otherwise} \end{cases} \tag{23}$$

where I_0 is the magnitude of the current, $\bar{\lambda}_0 = \lambda_0/(4\sqrt{\epsilon_{\text{eff}}})$ with $\lambda_0 = 2\pi/k_0$, $\phi_0 = w/(2b)$, $\hat{\boldsymbol{z}}$ is the unit vector along the z direction, and

$$\epsilon_{\text{eff}} = \frac{\epsilon_{r1} + 1}{2} + \frac{\epsilon_{r1} - 1}{2} \frac{1}{\sqrt{1 + 10\,(h/w)}} \tag{24}$$

as in [16, 17], with h being the thickness of the substrate.

The Fourier transform of this current is given by

$$\tilde{J}_{sz}(n, k_z) = \frac{I_0}{\pi b} \operatorname{sinc}\left(\frac{nw}{2b}\right) \frac{k_0 \sqrt{\epsilon_{\text{eff}}}}{k_0^2 \epsilon_{\text{eff}} - k_z^2} \cos\left(k_z \frac{\lambda_0}{4\sqrt{\epsilon_{\text{eff}}}}\right) \tag{25}$$

where $\operatorname{sinc}(x) = \sin(x)/x$.

Substituting for $\tilde{J}_{sz}(n, k_z)$ from (25) and $\tilde{J}_{s\phi}(n, k_z) = 0$ in (19)–(20), using the expressions of $A_{4n}(k_z)$ and $C_{4n}(k_z)$ so obtained in (21) and (22), respectively, noting that $M_{21}(-n, k_z) = (-1)^{n+1} M_{21}(n, k_z)$, $M_{22}(-n, k_z) = (-1)^n M_{22}(n, k_z)$, $\Delta(-n, k_z) = \Delta(n, k_z)$, and after simplifying, we can write the electric field components in the far zone as

$$\begin{aligned} E_\theta(r, \theta, \phi) \ &= \ -\frac{I_0}{\pi^2 (k_0 b) \sin\theta} \frac{e^{-jk_0 r}}{r} \frac{\sqrt{\epsilon_{\text{eff}}}}{\epsilon_{\text{eff}} - \cos^2\theta} \cos\left(\frac{\pi \cos\theta}{2\sqrt{\epsilon_{\text{eff}}}}\right) \\ &\quad \sum_{n=0}^{\infty} \varepsilon_n \, j^{n+1} \cos(n\phi) \operatorname{sinc}\left(\frac{nw}{2b}\right) \frac{M_{22}(n, k_0 \cos\theta)}{\Delta(n, k_0 \cos\theta)} \end{aligned} \tag{26}$$

$$\begin{aligned} E_\phi(r, \theta, \phi) \ &= \ \frac{I_0 \eta_0}{\pi^2 (k_0 b) \sin\theta} \frac{e^{-jk_0 r}}{r} \frac{\sqrt{\epsilon_{\text{eff}}}}{\epsilon_{\text{eff}} - \cos^2\theta} \cos\left(\frac{\pi \cos\theta}{2\sqrt{\epsilon_{\text{eff}}}}\right) \\ &\quad \sum_{n=0}^{\infty} \varepsilon_n \, j^{n} \sin(n\phi) \operatorname{sinc}\left(\frac{nw}{2b}\right) \frac{M_{21}(n, k_0 \cos\theta)}{\Delta(n, k_0 \cos\theta)} \end{aligned} \tag{27}$$

where $\varepsilon_n = 1$ for $n = 0$ and $\varepsilon_n = 2$ for $n > 0$.

3.2. Radiation from an Azimuthal Patch Antenna

In this case we consider the patch dimensions $2b\phi_0$ and $2L$ in Fig. 1 to be equal to half a wavelength and w, respectively, and the surface current $\boldsymbol{J}_s$ on the patch to be azimuthally directed. Assuming the variation of $\boldsymbol{J}_s$ with the z coordinate to be negligible, we can then write [11]

$$\boldsymbol{J}_s(\phi,z)=\begin{cases}\hat{\boldsymbol{\phi}}\dfrac{I_0}{w}\cos(k_0b\sqrt{\epsilon_{\text{eff}}}\phi), & -\dfrac{\bar{\lambda}_0}{b}\le\phi\le\dfrac{\bar{\lambda}_0}{b},\quad -\dfrac{w}{2}\le z\le\dfrac{w}{2}\\ 0, \quad \text{otherwise.}\end{cases} \tag{28}$$

The Fourier transform of this current is given by

$$\tilde{J}_{s\phi}(n,k_z)=\frac{I_0}{\pi b}\,\text{sinc}\left(\frac{k_zw}{2}\right)\frac{k_0\sqrt{\epsilon_{\text{eff}}}}{k_0^2\epsilon_{\text{eff}}-(n/b)^2}\cos\left(\frac{n}{b}\frac{\lambda_0}{4\sqrt{\epsilon_{\text{eff}}}}\right). \tag{29}$$

Substituting for $\tilde{J}_{s\phi}(n,k_z)$ from (29) and $\tilde{J}_{sz}(n,k_z)=0$ in (19)–(20), using the expressions of $A_{4n}(k_z)$ and $C_{4n}(k_z)$ so obtained in (21) and (22), respectively, noting that $M_{11}(-n,k_z)=(-1)^nM_{11}(n,k_z)$, $M_{12}(-n,k_z)=(-1)^{n+1}M_{12}(n,k_z)$, and after simplifying, we can write the electric field components in the far zone as

$$E_\theta(r,\theta,\phi)=-\frac{I_0}{\pi^2(k_0b)}\frac{e^{-jk_0r}}{r\sin\theta}\,\text{sinc}\left(\frac{k_0w}{2}\cos\theta\right)\sum_{n=0}^{\infty}\varepsilon_n\frac{j^n\sin(n\phi)\sqrt{\epsilon_{\text{eff}}}}{\epsilon_{\text{eff}}-\left(\dfrac{n}{k_0b}\right)^2}\cos\left(\frac{n\pi}{2k_0b\sqrt{\epsilon_{\text{eff}}}}\right)\frac{M_{12}(n,k_0\cos\theta)}{\Delta(n,k_0\cos\theta)} \tag{30}$$

$$E_\phi(r,\theta,\phi)=\frac{I_0\eta_0}{\pi^2(k_0b)}\frac{e^{-jk_0r}}{r\sin\theta}\,\text{sinc}\left(\frac{k_0w}{2}\cos\theta\right)\sum_{n=0}^{\infty}\varepsilon_n\frac{j^{n+1}\cos(n\phi)\sqrt{\epsilon_{\text{eff}}}}{\epsilon_{\text{eff}}-\left(\dfrac{n}{k_0b}\right)^2}\cos\left(\frac{n\pi}{2k_0b\sqrt{\epsilon_{\text{eff}}}}\right)\frac{M_{11}(n,k_0\cos\theta)}{\Delta(n,k_0\cos\theta)}. \tag{31}$$

3.3. Directivity

The directivity of an antenna in the direction θ,ϕ is given by

$$D(\theta,\phi)=\frac{4\pi P(\theta,\phi)}{\displaystyle\int_0^{2\pi}\int_0^{\pi}P(\theta,\phi)\sin\theta\,d\theta\,d\phi} \tag{32}$$

where $P(\theta,\phi)$ is the power radiated per unit solid angle in the direction θ,ϕ which can be written in terms of the θ and ϕ components of the electric field in the far zone as

$$P(\theta,\phi) = \frac{r^2}{2\eta_0}\,\mathrm{Re}[E_\theta(r,\theta,\phi)E_\theta^*(r,\theta,\phi) + E_\phi(r,\theta,\phi)E_\phi^*(r,\theta,\phi)] \quad (33)$$

with the asterisk denoting the complex conjugate and $\mathrm{Re}[\mathcal{Z}]$ denoting the real part of the complex number $\mathcal{Z}$. Substituting from (26) and (27) in (33), for the axial patch antenna we can write

$$P(\theta,\phi) = \frac{I_0^2}{2\pi^4\eta_0(k_0b)^2\sin^2\theta}\left(\frac{\sqrt{\epsilon_{\mathrm{eff}}}}{\epsilon_{\mathrm{eff}}-\cos^2\theta}\right)^2\cos^2\left(\frac{\pi\cos\theta}{2\sqrt{\epsilon_{\mathrm{eff}}}}\right)$$
$$\mathrm{Re}\left\{\sum_{n=0}^{\infty}\sum_{v=0}^{\infty}\varepsilon_n\varepsilon_v\,j^{n-v}\,\mathrm{sinc}\left(\frac{nw}{2b}\right)\mathrm{sinc}\left(\frac{vw}{2b}\right)\Psi_{nv}(\theta,\phi)\right\} \quad (34)$$

where

$$\Psi_{nv}(\theta,\phi) = \mathcal{M}_{22}(n,\theta)\mathcal{M}_{22}^*(v,\theta)\cos(n\phi)\cos(v\phi)$$
$$+\eta_0^2\,\mathcal{M}_{21}(n,\theta)\mathcal{M}_{21}^*(v,\theta)\sin(n\phi)\sin(v\phi) \quad (35)$$

with $\mathcal{M}_{2i}(u,\theta)$ denoting $M_{2i}(u,k_0\cos\theta)/\Delta(u,k_0\cos\theta)$ for $i=1,2$. Integrating both sides of (34) over θ from 0 to π and over ϕ from 0 to 2π yields

$$\int_0^{2\pi}\int_0^{\pi}P(\theta,\phi)\sin\theta\,d\theta\,d\phi = \frac{2\pi I_0^2}{2\pi^4\eta_0(k_0b)^2}\sum_{n=0}^{\infty}\varepsilon_n\,\mathrm{sinc}^2\left(\frac{nw}{2b}\right)\mathcal{I}_n \quad (36)$$

where

$$\mathcal{I}_n = \int_0^{\pi}\left\{\frac{|\mathcal{M}_{22}(n,\theta)|^2+\eta_0^2(1-\delta_{n0})|\mathcal{M}_{21}(n,\theta)|^2}{\sin\theta}\right\}$$
$$\left(\frac{\sqrt{\epsilon_{\mathrm{eff}}}}{\epsilon_{\mathrm{eff}}-\cos^2\theta}\right)^2\cos^2\left(\frac{\pi\cos\theta}{2\sqrt{\epsilon_{\mathrm{eff}}}}\right)d\theta \quad (37)$$

with δ_{n0} being the Kronecker delta. Explicit expressions similar to those in (34) and (36) can be obtained for the azimuthal patch antenna also by substituting in (33) from (30) and (31), and then integrating the resulting expression over θ and ϕ.

4. RESULTS

Results are presented as plots of normalized radiation patterns in the horizontal plane ($\theta = 90^\circ$) versus the azimuth angle (ϕ) for both axial

and azimuthal patch antennas, and also as plots of directivity versus the elevation angle (θ) in the $\phi = 90^\circ$ plane, for the axial patch antenna.

We have verified that our analysis and the software written for performing the analysis are correct by reproducing the results in Figs. 3–5 and Figs. 7–8 of [10] as well as those in Figs. 2 and 4 of [11], by substituting $d = c = b$ in the software used for calculating the radiation patterns and the directivity. Fig. 2 shows the reproduced results in Fig. 3 of [10] for $a = 0.25\lambda_0$ and $h = 0.05\lambda_0$.

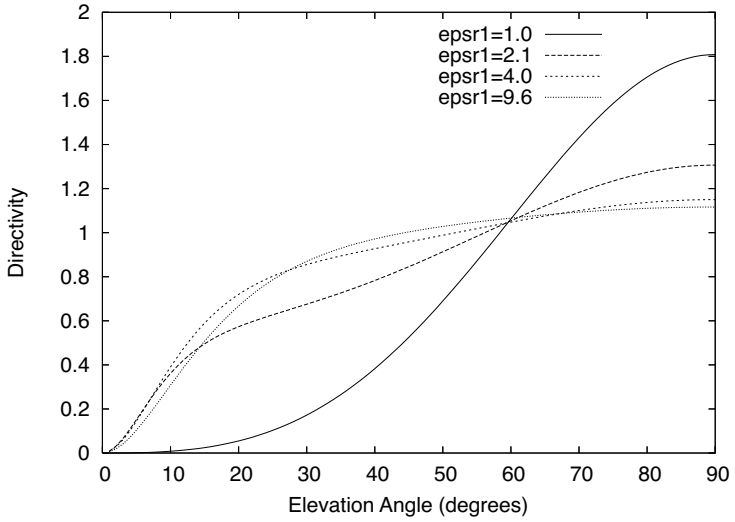

Figure 2. Plot of directivity versus elevation angle for a wraparound antenna with $a = 0.25\lambda_0$ and $h = 0.05\lambda_0$, for different substrate relative permittivities ϵ_{r1}.

We have calculated results for a cylindrical-rectangular microstrip patch antenna of dimensions $a = 5\lambda_0$, $h = 0.006a$, $w = 0.04a$, with a substrate of relative permittivity $\epsilon_{r1} = 2.2$ and a superstrate of thickness $0.06a$. When performing calculations, retaining 50 terms in the infinite series associated with E_θ and E_ϕ has been sufficient to get a four significant digit accuracy in the calculated results. The same accuracy can be obtained with a lesser number of terms, when the antenna dimensions are smaller. From the numerical experiments performed we have found that when $a = 3\lambda_0$ and $a = \lambda_0$, retaining 30 and 20 terms respectively, is sufficient to obtain a four significant digit accuracy in the calculated results. The calculations were done in a SunFire 880 Solaris 8 UNIX server and took only 10 seconds of CPU time on the average for calculation of the normalized patterns such as

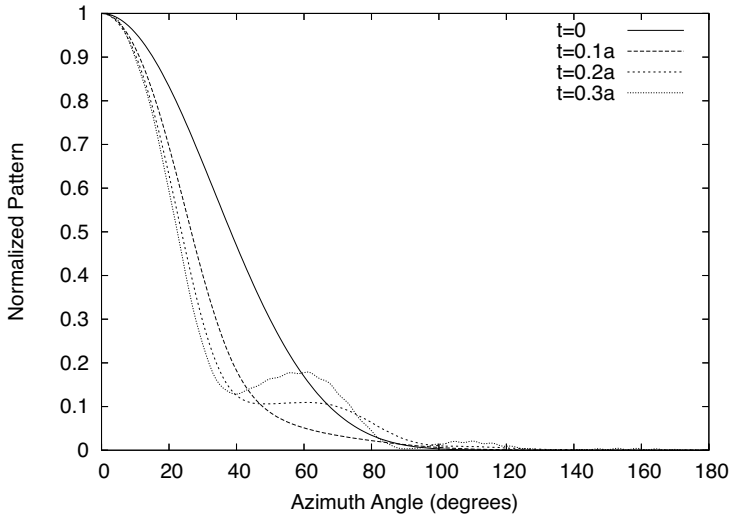

Figure 3. Variation of the normalized pattern with the azimuth angle for a cylindrical-rectangular microstrip antenna loaded with an air gap and a superstrate, with $a = 5\lambda_0$, $h = 0.006a$, $w = 0.04a$, $d - c = 0.06a$, $\epsilon_{r1} = 2.2$, and an axial patch, for various thicknesses ($t = c - b$ in wavelengths) of the air gap, when the relative permittivity ϵ_{r3} of the superstrate is 4.0.

those in Fig. 3 for all four thicknesses of the air gap.

The plots in Fig. 3 show how the normalized radiation pattern varies with the thickness of the air gap for a cylindrical-rectangular axial patch antenna loaded with an air gap and a superstrate made of a lossless material of relative permittivity $\epsilon_{r3} = 4.0$. Fig. 4 shows the corresponding plots for a similar configuration when the superstrate is made of a lossy material of relative permittivity $\epsilon_{r3} = 4.0 - j0.5$. As can be seen from the plots, for each air gap thickness, the introduction of the loss broadens the pattern in the main lobe region without causing any significant change to the pattern outside this region. Also we can observe a narrowing of the main lobes of the patterns in both Figs. 3 and 4, as the thickness of the air gap t is increased from 0 to $1.5\lambda_0$.

The plots in Figs. 5 and 6 show how the normalized radiation pattern varies with the thickness of the air gap, for a cylindrical-rectangular azimuthal patch antenna loaded with an air gap and superstrates made of lossless and lossy materials of relative permittivities $\epsilon_{r3} = 4.0$ and $\epsilon_{r3} = 4.0 - j0.5$, respectively. When there is no air gap ($t = 0$), the patterns for the azimuthal patch antenna are much

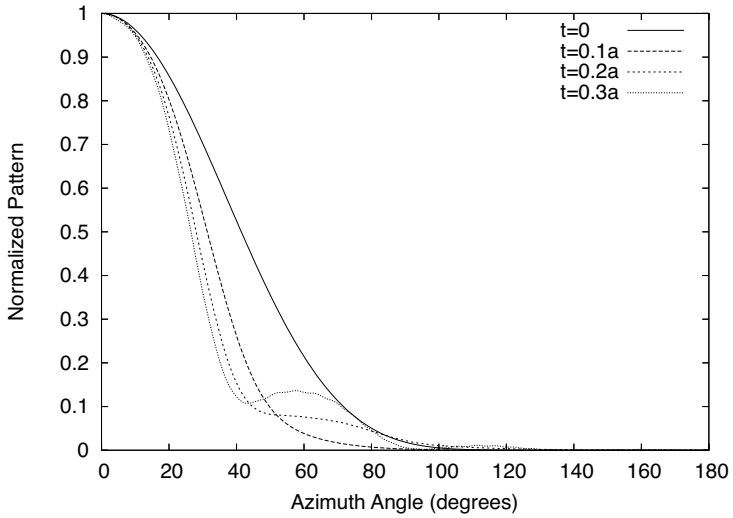

Figure 4. Variation of the normalized pattern with the azimuth angle for the antenna considered in Fig. 3 for various thicknesses ($t = c - b$ in wavelengths) of the air gap, when $\epsilon_{r3} = 4.0 - j0.5$.

narrower than the corresponding patterns for the axial patch antenna, in the main lobe region. However, when there is an air gap, for a particular thickness of the air gap, the patterns of both antennas for each value of ϵ_{r3} are almost the same in the main lobe region, but the sidelobe levels of the azimuthal patch antenna are significantly higher than those of the axial patch antenna. The main lobes of the patterns in Figs. 5 and 6 also become narrower as the thickness of the air gap is increased from 0 to $1.5\lambda_0$.

Fig. 7 shows the behavior of the patterns in response to a change in the lossyness of the superstrate material for the axial patch antenna considered in Figs. 3 and 4, when the air gap thickness is held constant at $1.5\lambda_0$. It can clearly be seen from these plots the broadening of the main lobes of the patterns with the increasing lossyness of the superstrate material. A similar behavior of patterns can be observed for the azimuthal patch antenna also, but with higher sidelobe levels than that for the axial patch antenna, for a particular value of ϵ_{r3}.

Finally, Fig. 8 shows how the directivity of the axial patch antenna considered in Fig. 4 changes with the elevation angle in the $\phi = 90^\circ$ plane, for different thicknesses t of the air gap. From these patterns we can see that the directivity of the antenna increases with t. In all of the above figures, ripples appear on the plots as the size of the air

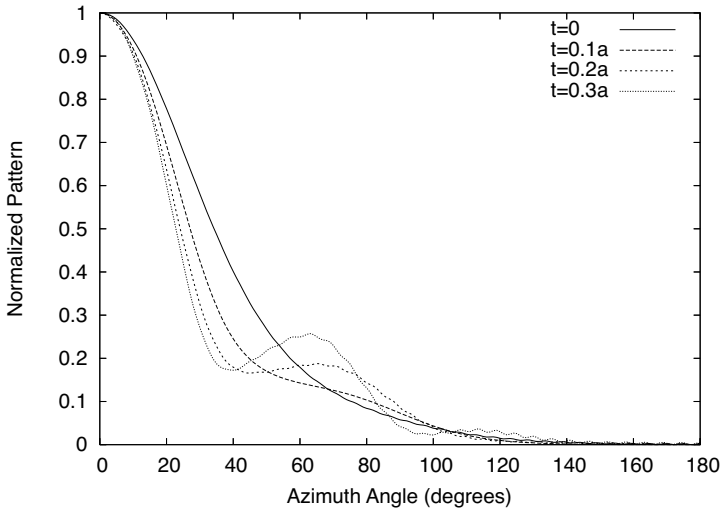

Figure 5. Variation of the normalized pattern with the azimuth angle for a cylindrical-rectangular microstrip antenna loaded with an air gap and a superstrate, with $a = 5\lambda_0$, $h = 0.006a$, $w = 0.04a$, $d - c = 0.06a$, $\epsilon_{r1} = 2.2$, and an azimuthal patch, for various thicknesses ($t = c - b$ in wavelengths) of the air gap, when the relative permittivity ϵ_{r3} of the superstrate is 4.0.

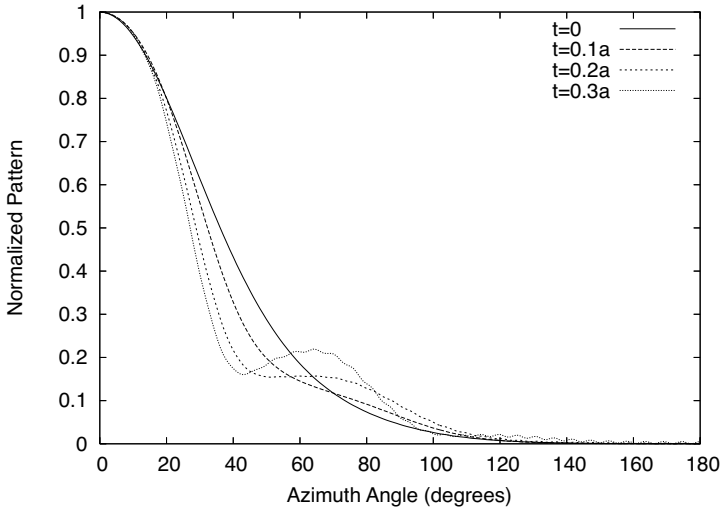

Figure 6. Variation of the normalized pattern with the azimuth angle for the antenna considered in Fig. 5 for various thicknesses ($t = c - b$ in wavelengths) of the air gap, when $\epsilon_{r3} = 4.0 - j0.5$.

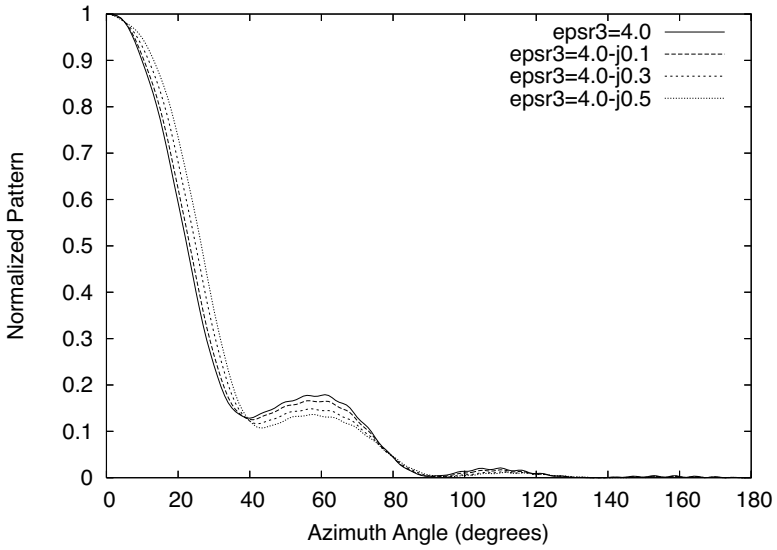

Figure 7. Variation of the normalized pattern with the azimuth angle for the antenna considered in Figs. 3 and 4, for various values of the superstrate relative permittivity ϵ_{r3}, when the air gap thickness is held constant at $1.5\lambda_0$.

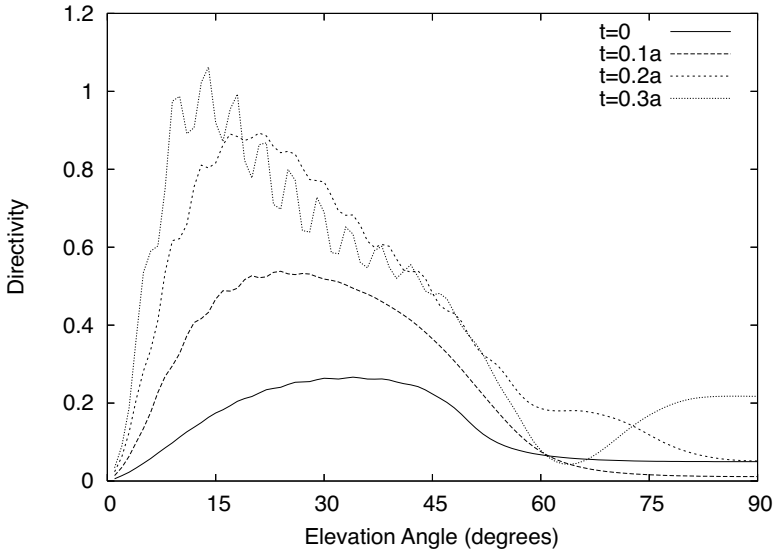

Figure 8. Variation of the directivity in the $\phi = 90^\circ$ plane with the elevation angle for the antenna considered in Fig. 4, for various thicknesses of the air gap $t = c - b$ in wavelengths.

gap t increases from 0 to $1.5\lambda_0$. This is due to the interference caused by reflections. These ripples are more prominent for $t \geq \lambda_0$.

5. CONCLUSION

A cylindrical-rectangular microstrip patch antenna loaded with a superstrate and an air gap between the substrate and the superstrate has been analyzed using the ESCM. Results have been presented in the form of normalized radiation patterns for both axial and azimuthal patch antennas and also as directivity patterns for an axial patch antenna, for superstrates made of lossless and lossy dielectric material. This is the first time such a structure has been comprehensively analyzed using the ESCM. From the results obtained it is clear that the thickness of the air gap and the loss of the superstrate material has a significant effect on the radiation from these antennas.

APPENDIX A. COEFFICIENTS ASSOCIATED WITH EQUATIONS (9) TO (12)

The coefficients σ_i^e, τ_i^e, α_i^e, β_i^e, for $i = 1, 2, 3$ and $e = a, c$ associated with (9)–(12) are given below.

$$\sigma_3^a = -\alpha_0 \frac{nk_z}{j\omega\mu_0 k_{3\rho} d}\left(1 - \frac{k_{3\rho}^2}{k_{4\rho}^2}\right) \tag{A1}$$

$$\sigma_3^c = \alpha_0 \left[\frac{k_{3\rho}}{k_{4\rho}} \frac{H_n^{(2)'}(k_{4\rho}d)}{H_n^{(2)}(k_{4\rho}d)} - \frac{J_n'(k_{3\rho}d)}{J_n(k_{3\rho}d)}\right] \tag{A2}$$

with

$$\alpha_0 = \frac{j\pi k_{3\rho} d}{2} J_n(k_{3\rho}d) H_n^{(2)}(k_{4\rho}d). \tag{A3}$$

$$\tau_3^a = -\frac{\sigma_3^a H_n^{(2)}(k_{3\rho}d)}{J_n(k_{3\rho}d)} \tag{A4}$$

$$\tau_3^c = \frac{H_n^{(2)}(k_{4\rho}d) - \sigma_3^c H_n^{(2)}(k_{3\rho}d)}{J_n(k_{3\rho}d)} \tag{A5}$$

$$\alpha_3^a = \alpha_0 \left[\frac{k_{3\rho}\epsilon_{r4}}{k_{4\rho}\epsilon_{r3}} \frac{H_n^{(2)'}(k_{4\rho}d)}{H_n^{(2)}(k_{4\rho}d)} - \frac{J_n'(k_{3\rho}d)}{J_n(k_{3\rho}d)}\right] \tag{A6}$$

$$\alpha_3^c = \alpha_0 \frac{nk_z}{j\omega\epsilon_3 k_{3\rho} d}\left(1 - \frac{k_{3\rho}^2}{k_{4\rho}^2}\right) \tag{A7}$$

$$\beta_3^a = \frac{H_n^{(2)}(k_{4\rho}d) - \alpha_3^a H_n^{(2)}(k_{3\rho}d)}{J_n(k_{3\rho}d)} \tag{A8}$$

$$\beta_3^c = -\frac{\alpha_3^c H_n^{(2)}(k_{3\rho}d)}{J_n(k_{3\rho}d)} \tag{A9}$$

$$\begin{aligned}\alpha_2^e = {} & \frac{n\pi k_z}{2\omega\epsilon_2}\left(1-\frac{k_{2\rho}^2}{k_{3\rho}^2}\right)[\sigma_3^e H_n^{(2)}(k_{3\rho}c)+\tau_3^e J_n(k_{3\rho}c)]J_n(k_{2\rho}c) \\ & +\frac{j\pi k_{2\rho}c}{2}\left\{\frac{k_{2\rho}\epsilon_{r3}}{k_{3\rho}\epsilon_{r2}}[\alpha_3^e H_n^{(2)'}(k_{3\rho}c)+\beta_3^e J_n'(k_{3\rho}c)]J_n(k_{2\rho}c)\right. \\ & \left.-[\alpha_3^e H_n^{(2)}(k_{3\rho}c)+\beta_3^e J_n(k_{3\rho}c)]J_n'(k_{2\rho}c)\right\}\end{aligned} \tag{A10}$$

$$\begin{aligned}\sigma_2^e = {} & -\frac{n\pi k_z}{2\omega\mu_0}\left(1-\frac{k_{2\rho}^2}{k_{3\rho}^2}\right)[\alpha_3^e H_n^{(2)}(k_{3\rho}c)+\beta_3^e J_n(k_{3\rho}c)]J_n(k_{2\rho}c) \\ & +\frac{j\pi k_{2\rho}c}{2}\left\{\frac{k_{2\rho}}{k_{3\rho}}[\sigma_3^e H_n^{(2)'}(k_{3\rho}c)+\tau_3^e J_n'(k_{3\rho}c)]J_n(k_{2\rho}c)\right. \\ & \left.-[\sigma_3^e H_n^{(2)}(k_{3\rho}c)+\tau_3^e J_n(k_{3\rho}c)]J_n'(k_{2\rho}c)\right\}.\end{aligned} \tag{A11}$$

Explicit expressions of β_2^e and τ_2^e are obtained from those of α_2^e and σ_2^e, respectively, by replacing $J_n(k_{2\rho}c)$ by $-H_n^{(2)}(k_{2\rho}c)$ and $J_n'(k_{2\rho}c)$ by $-H_n^{(2)'}(k_{2\rho}c)$.

$$\alpha_1^e = \frac{[\alpha_2^e H_n^{(2)}(k_{2\rho}b)+\beta_2^e J_n(k_{2\rho}b)]J_n(k_{1\rho}a)}{J_n(k_{1\rho}a)H_n^{(2)}(k_{1\rho}b) - J_n(k_{1\rho}b)H_n^{(2)}(k_{1\rho}a)} \tag{A12}$$

$$\begin{aligned}\sigma_1^e = {} & \frac{[\sigma_2^e H_n^{(2)'}(k_{2\rho}b)+\tau_2^e J_n'(k_{2\rho}b)]k_{1\rho}J_n'(k_{1\rho}a)}{[J_n'(k_{1\rho}a)H_n^{(2)'}(k_{1\rho}b) - J_n'(k_{1\rho}b)H_n^{(2)'}(k_{1\rho}a)]k_{2\rho}} - \frac{nk_z}{j\omega\mu_0 k_{1\rho}b} \\ & \left(1-\frac{k_{\rho1}^2}{k_{\rho2}^2}\right)\frac{[\alpha_2^e H_n^{(2)}(k_{2\rho}b)+\beta_2^e J_n(k_{2\rho}b)]J_n'(k_{1\rho}a)}{J_n'(k_{1\rho}a)H_n^{(2)'}(k_{1\rho}b) - J_n'(k_{1\rho}b)H_n^{(2)'}(k_{1\rho}a)}.\end{aligned} \tag{A13}$$

Explicit expressions of β_1^e and τ_1^e are obtained from those of α_1^e and σ_1^e, respectively, by replacing $J_n(k_{1\rho}a)$ and $J_n'(k_{1\rho}a)$ in the numerators by $-H_n^{(2)}(k_{1\rho}a)$ and $-H_n^{(2)'}(k_{1\rho}a)$, respectively.

REFERENCES

1. Luk, K. M., K. F. Lee, and J. S. Dahele, "Analysis of the cylindrical-rectangular patch antenna," *IEEE Trans. Antennas Propagat.*, Vol. 37, No. 2, 143–147, Feb. 1989.
2. Heckler, M. V. T., M. Bonadiman, R. Schildberg, L. Cividanes, and J. C. S. Lacava, "CAD package to design rectangular probe-fed microstrip antennas conformed on cylindrical structures," *Proc. SBMO/IEEE MTT-S Int. Microwave and Optoelectronics Conf.*, Vol. 2, 747–752, 2003.
3. Ali, S. M., T. M. Habashy, J. F. Kiang, and J. A. Kong, "Resonance in cylindrical-rectangular and wraparound structures," *IEEE Trans. Microwave Theory Tech.*, Vol. 37, No. 11, 1773–1783, Nov. 1989.
4. Habashy, T. M., S. M. Ali, and J. A. Kong, "Input impedance and radiation pattern of cylindrical-rectangular and wraparound microstrip antennas," *IEEE Trans. Antennas Propagat.*, Vol. 38, No. 5, 722–731, May 1990.
5. Li, L. W., T. X. Zhao, M. S. Leong, and T. S. Yeo, "A spatial domain method of moments analysis of a cylindrical-rectangular chirostrip," *Progress In Electromagnetics Research*, PIER 35, 165–182, 2002.
6. Yin, W. and W. Wang, "Dyadic Green's function of cylindrical multilayered chiral media and its applications," *J. Electromagn. Waves Applic.*, Vol. 7, No. 7, 1005–1027, 1993.
7. Li, L. W., P. S. Kooi, M. S. Leong, and T. S. Yeo, "Analytic representation of scattering dyadic Green's functions coefficients for cylindrically multilayered chiral media," *J. Electromagn. Waves Applic.*, Vol. 9, No. 9, 1207–1221, 1995.
8. Silva, F. D. C., S. B. Fonseca, A. J. M. Soares, and A. J. Giarola, "Analysis of microstrip antennas on circular-cylindrical substrates with a dielectric overlay," *IEEE Trans. Antennas Propagat.*, Vol. 39, No. 9, 1398–1404, Sept. 1991.
9. Wong, K. L., Y. T. Cheng, and J. S. Row, "Resonance in a superstrate-loaded cylindrical-rectangular microstrip structure," *IEEE Trans. Microwave Theory Tech.*, Vol. 41, No. 5, 814–819, May 1993.
10. Ashkenazy, J., S. Shtrikman, and D. Treves, "Electric surface current model for the analysis of microstrip antennas on cylindrical bodies," *IEEE Trans. Antennas Propagat.*, Vol. 33, No. 3, 295–300, Mar. 1985.

11. Ashkenazy, J., S. Shtrikman, and D. Treves, "Radiation patterns of half-wavelength microstrip elements on cylindrical bodies," *Proc. IEEE AP-S Int. Symp.*, Vol. 23, No. 1, 401–404, 1985.
12. Oliveira, F. S., K. C. Barbosa, and O. M. C. Pereira-Filho, "Analysis of superstrate loaded cylindrical-rectangular microstrip antennas using the electric surface current method," *Proc. SBMO/IEEE MTT-S Int. Microwave and Optoelectronics Conf.*, 657–660, 2005.
13. Harrington, R. F., *Time Harmonic Electromagnetic Fields*, McGraw-Hill, New York, 1961.
14. Zhang, K. and D. Li, *Electromagnetic Theory for Microwaves and Optoelectronics*, Springer-Verlag, New York, 1998.
15. Tai, C. T., *Dyadic Green's Functions in Electromagnetic Theory*, Intertext, New York, 1971.
16. Schneider, M. V., "Microstrip dispersion," *Proc. IEEE*, Vol. 60, No. 1, 144–146, 1972.
17. Schneider, M. V., "Microstrip lines for microwave integrated circuits," *Bell Syst. Tech. J.*, Vol. 48, 1421–1444, 1969.